J Electroceram (2016) 37:127–136
DOI 10.1007/s10832-016-0049-7

Electrical and mechanical properties of MgO added $0.5Ba(Zr_{0.2}Ti_{0.8})O_3$–$0.5(Ba_{0.7}Ca_{0.3})TiO_3$ (BZT–0.5BCT) composite ceramics

P. Adhikari[1] · **R. Mazumder**[1] · **S. Abhinay**[1]

Received: 26 April 2016 / Accepted: 4 July 2016 / Published online: 11 July 2016

Abstract MgO (0–2.0 vol%) added $Ba(Zr_{0.2}Ti_{0.8})O_3$–$0.5(Ba_{0.7}Ca_{0.3})TiO_3$ (BZT-0.5BCT) ceramics have been prepared by the conventional solid-state reaction method. The effects of MgO powder on the phase formation, densification, dielectric, piezoelectric and mechanical properties (flexural strength, hardness) of the BZT-0.5BCT ceramics have been studied systematically. The synthesized powder could be densified to 97 % of true density at a temperature of 1350 °C. The MgO addition also provided materials with better mechanical properties. The most interesting aspect of MgO added samples is their relative permittivity vs. temperature response. MgO additions effectively suppress the relative permittivity around phase transition temperature. The aging rate of d_{33} observed for BZT-0.5BCT is 14 %/decade. MgO addition reduces the ageing rate and for 1 vol% MgO added, BZT-0.5BCT shows aging rate of 3 %/decade. BZT-0.5BCT/MgO ceramics possesses good mechanical properties viz., flexural strength 93 MPa, which is almost 25 % higher than that of monolithic BZT-0.5BCT (73 MPa).

Keywords Lead free ferroelectric ceramics · BZT-0.5BCT · Sintering temperature · Dielectric constant · Flexural strength

1 Introduction

Lead based perovskite ferroelectric materials are widely used in multilayer capacitors, thermal imaging, actuators, piezoelectric transducers and ferroelectric memories because of its excellent ferroelectric and piezoelectric properties. The primary compositions in commercial use for piezoelectric applications are lead zirconate titanate (PZT) of compositions close to morphotropic phase boundary between rhombohedral and tetragonal phases [$Pb(Zr_{0.52}Ti_{0.48})O_3$] [1–3]. However, the recent concern about environmental pollution and toxicity of lead based materials have generated renewed interest in developing lead free piezoelectric ceramics to replace the lead- based ceramics. Therefore, tremendous efforts have been devoted in last decade to the development of competitive lead free counterparts, such as $BaTiO_3$, $(Bi_{1/2}Na_{1/2})TiO_3$ (BNT), (K, Na)NbO_3 (KNN), and their derivatives [4–9]. KNN based system suffers from alkali evaporation during sintering, poor sinterability, moisture sensitivity of the raw materials. BNT based system suffers from high leakage current.

Recently, Liu and Ren [10] have reported that Pb-free $Ba(Zr_{0.2}Ti_{0.8})O_3$–0.5 $(Ba_{0.7}Ca_{0.3})TiO_3$ (BZT-0.5BCT) solid solution exhibits high piezoelectric coefficient (d_{33} = 300-600 pC/N) near the tricritical point at room temperature which is superior to PZT based system. There are many reports available on the improvement of the dielectric and piezoelectric properties of BZT-0.5BCT by varying the synthesis and the sintering conditions [11–13]. It is to be mentioned that the electrical and mechanical properties, both are important for above mentioned applications. The electrical properties of BZT- 0.5BCT solid solutions have been studied extensively; however most of the work focuses on the nature of phase transition, structure, powder synthesis, the effect of processing condition on dielectric and piezoelectric properties and the temperature dependence of the dielectric and piezoelectric properties [10–13]. However, there are very few reports [14, 15] available on the study of mechanical properties of BZT-0.5BCT and no reports on its improvement with different techniques. $BaTiO_3$-based ceramics suffers from low

✉ R. Mazumder
ranabrata@nitrkl.ac.in; rana_brata@hotmail.com

[1] Department of Ceramic Engineering, National Institute of Technology, Rourkela, Odisha 769008, India

reliability and poor mechanical properties such as fracture strength and toughness [16]. To use it for electronic components, not only its dielectric properties but also its mechanical properties are important. For example, a stress of 30–50 MPa is generated in the capacitor/actuator during end termination and soldering.

A novel method has been used to improve the mechanical properties of structural ceramics and ferroelectrics by reinforcement of oxide (Al_2O_3, MgO, and ZrO_2) or non-oxide (SiC) particles and in some cases metal particles [17–19]. It is well known that electrical properties of ferroelectric ceramics degrade with non-ferroelectric additives and decrease in sinterability usually encountered with refractory oxide additives. Use of nano-oxide additives may drastically reduce the amount of additive, and the electrical properties may not degrade much. There are many reports available on mechanical and piezoelectric properties of the PZT-based system with different additives with an aim to improve the mechanical properties without losing electrical properties much. Tajima et al. [20] showed that it is possible to increase the fracture toughness (1.7 times higher than normal PZT ceramics) of PZT-based nano-composites with various oxides (Al_2O_3, MgO, and ZrO_2). Jiansirisomboon et al. [21] studied the effect of nano-sized NiO addition (i.e. 0, 0.1, 0.5 and 1 wt%) on structure and densification of PZT/NiO nano composite. The addition of NiO was found to improve hardness and only slightly affects fracture toughness. Zeng et al. [22] fabricated the SiC reinforced PZT ceramics by diffusing SiC at different times. Fracture strength and Young's modulus increased with the diffusion time of SiC. The increment could be attributed to the diffusion of SiC into the microscopic pores, cracks and grain boundary of PZT ceramics. Xiang et al. [23] reported the improvement of fracture strength and fracture toughness of the PZT ceramics with 0.1 wt% Y_2O_3 additions.

Adhikari et al. [24] reported the effect of nano-sized Al_2O_3 addition on phase formation, densification, dielectric, piezoelectric and mechanical properties of BZT-0.5BCT. They observed that BZT-0.5BCT/Al_2O_3 ceramics possesses good mechanical properties viz., flexural strength of 92 MPa compared with pure BZT-0.5BCT (74 MPa) ceramics. Ren et al. [25] studied the effect of MgO (10 wt%–40 wt%) content on tunable dielectric properties of BZT/MgO composite. It was found that addition of MgO led to decrease in dielectric permittivity and Curie temperature to below 100 °C as a trace amount of Mg^{2+} ions dissolved in BZT grains. However, the addition of MgO helped in the increase in tunability by about 30 %. Nagai et al. [26] reported the effect of MgO doping (0.2–5 mol%) on the phase transformation of $BaTiO_3$ (BT). There was a decrease in the value of T_c (ΔT_c = 42 °C) with an increase in MgO content from 0.2 mol% to 2 mol%. Raman spectra revealed that orthorhombic phase is the stable phase at room temperature for 0.5 mol% MgO addition. Yoon et al. [27] studied the effect of liquid phase (MgO in the acceptor site of BT) characteristics on the microstructure and dielectric properties of BT. They reported that sintered density of about ~95 % were obtained with doping at acceptor site. It was observed that grain growth is critically affected by the liquid phase that formed during heat treatment. Vittayakorn et al. [28] reported the effect of nano-sized MgO particles (0–1 vol%) on the microstructural characterization and electrical properties of BT. The average grain size decreased from ~75 μm in pure BT to 0.4 μm in BT/MgO composite. MgO addition leads to grain growth suppression and poor densification. The dielectric constant decreased from ~5776 in dense BT to ~1956 in 1 vol% MgO content in BT/MgO nanocomposite.

To the best of our knowledge, there is no report available on electrical and mechanical properties of BZT-0.5BCT ceramics with the addition of nano-sized MgO with an aim to improve the mechanical property with suppression of permittivity peak height around the phase transition temperature. The present paper studied the effect of MgO addition on the phase evolution, densification, microstructure, dielectric, piezoelectric and mechanical properties of BZT–0.5BCT ceramics with an aim to improve the mechanical properties, stability of the electrical properties with temperature and time.

2 Experimental

BZT-0.5BCT [$Ba(Zr_{0.2}Ti_{0.8})O_3$–$0.5(Ba_{0.7}Ca_{0.3})TiO_3$] powders were prepared by solid state reaction method. The stoichiometric amount of $BaCO_3$ (99 %, Aldrich), ZrO_2 (99 %, Aldrich), TiO_2 (99 %, Aldrich), and $CaCO_3$ (99 %, Aldrich) powders were mixed using planetary mill (Fritsch Pulveriser) for 10 h (RPM-300) with zirconia ball and isopropyl alcohol as the media. The mixed powder was calcined at 1200 °C for 4 h. MgO powder (Sigma-Aldrich Chemie, GmbH) was mixed (after dispersing in acetone) with pure BZT-0.5BCT in a mortar pestle. Pellets from the synthesized powders were prepared using uniaxial pressing at a pressure of 350 MPa. The pellets were sintered at 1300-1350°C for 4 h in an air atmosphere and cooled in the furnace. The phase and crystal structure of all the samples were characterized using an X-ray diffraction analysis [RIGAKU/ULTIMA-IV] with a Cu Kα radiation (1.54178 A°). The particle morphology and microstructure of the sintered samples was characterized using field emission scanning electron microscope (FESEM) [NOVA NANOSEM 450]. Density of the sintered sample was measured by Archimedes principle. For dielectric measurement, the surfaces of the sintered pellets were polished followed by application of a silver conducting paste on two opposite surfaces of the sample. The silver paste was then cured at 500 °C for 30 min. The relative permittivity (ε_r), dissipation factor (tan δ) and impedance were measured using HIOKI 3532–50 LCR

Hitester. Ferroelectric hysteresis loops were obtained for unpoled samples at room temperature using a modified Sawyer-Tower circuit. The piezoelectric strain constant (d_{33}) was measured on a d_{33} meter (APCYE2730A d_{33} tester) after poling the samples in silicone oil at room temperature at 2.5 kV/mm field for 20 min. Flexural strength was determined in three-point bending as per ASTM standard C1161–90 [29] in UTM (Hounsfield H10KS, U.K). For three point bending, the span length was 40 mm and cross head speed was 0.5 mm/min. The flexural strength was calculated from the following equation [29]

$$\sigma_f = \frac{3FL}{2bd^2}$$

Where, F is the load (force) at the fracture point (N), L is the length of the support span (mm), b is width (mm) and d is thickness (mm). Macro-hardness was measured by the indentation technique using Vickers diamond indenter. The indentation load of 0.5 kg was applied for 10s.

3 Results and discussion

Figure.1 (a) shows the FESEM micrograph of the BZT-0.5BCT powder calcined at 1200 °C. BZT-0.5BCT powders are almost non-agglomerated and spherical to irregular in shape with a particle size in the range of 0.4 – 0.8 μm. The FESEM micrograph [Fig. 1(b)] depicts the particle size of MgO powder, which is in the range of 42 – 120 nm

Figure 2 (a) shows the X-ray diffraction patterns of nano-MgO (0–2 vol%) added BZT-0.5BCT ceramics sintered at 1350 °C /4 h. It can be observed that all compositions exhibit the perovskite structure. The diffraction pattern of pure BZT-0.5BCT ceramic (0 % MgO) matches with tetragonal perovskite $BaTiO_3$ (JCPDS file no. 75–0460), with lattice parameters a = 3.9945 Å and c = 4.0335 Å and space group P4/mmm. It is to be noted that $CaTiO_3$ secondary phase was generated for a small addition of MgO (0.5 vol%). The secondary phase of $Mg_2Zr_5O_{12}$ (JCPDS file no. 80–0967) can be observed at higher vol% of MgO (x > 1 vol%). No trace of MgO was detected, possibly because its amount was less than the XRD detection limit. Moreover, it is clear from the magnified X-ray pattern in the range of 65.5-67^o (Fig. 2 (b)) that the position of the diffraction peaks shift towards the lower diffraction angles with the addition of MgO indicating higher lattice volume. It is interesting to mention that (202) peak splitting was not disappeared with MgO addition but X-ray diffraction peaks are broadened. From the broadened X-ray profile, it is hard to acquire further information on the structural change of the composite upon MgO addition. For small addition of MgO in BZT-0.5BCT, Mg^{2+} incorporates into the

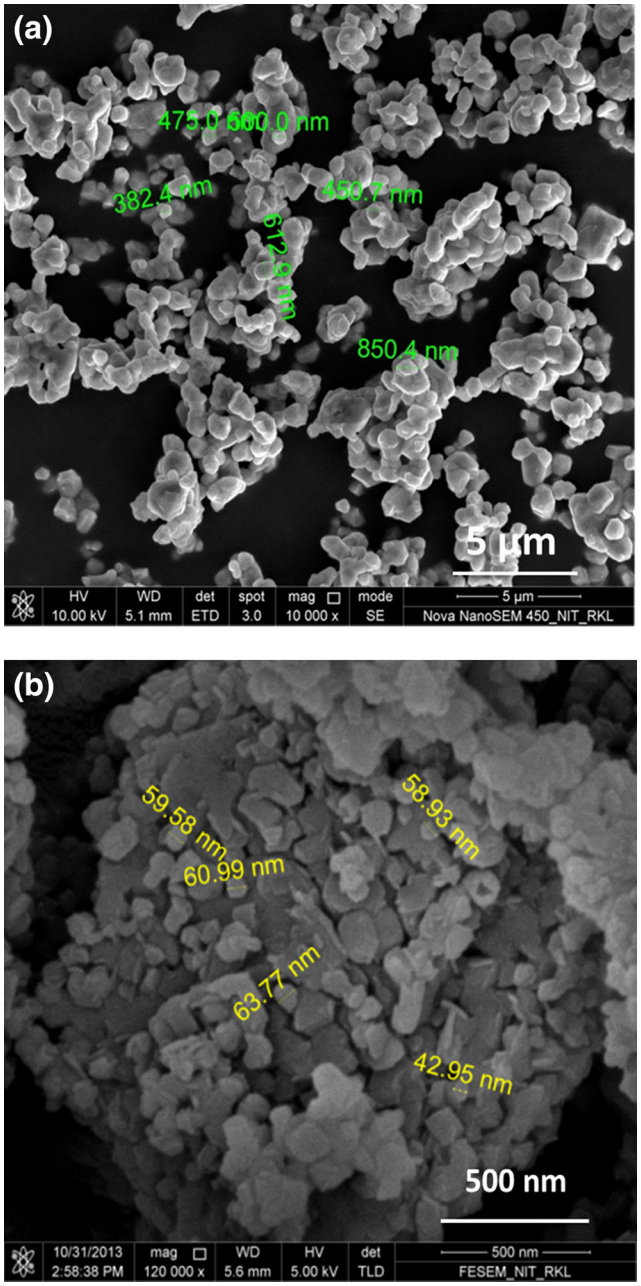

Fig. 1 FESEM micrograph of (**a**) BZT-0.5 BCT (**b**) MgO powder

B-site as acceptor dopant, and this can promote oxygen vacancies in the structure. As Mg^{2+} (0.72 Å) [24] have higher ionic radius compared to Ti^{4+} (0.605 Å), it increases the lattice parameter which is demonstrated in peak shifting to lower angle. Probably, incorporation of Mg^{2+} in BZT-0.5BCT destabilizes the structure and also expelled out less soluble Ca^{2+} ion which reacts with TiO_2 to form $CaTiO_3$. It may also create compositional inhomogeneity in the structure. That is also demonstrated later in the $\varepsilon_r \sim T$ plot. For higher addition, Zr comes out from the structure, and it reacts with excess MgO to form $Mg_2Zr_5O_{12}$ as MgO has only 1 atom% solubility in $BaTiO_3$ [30]

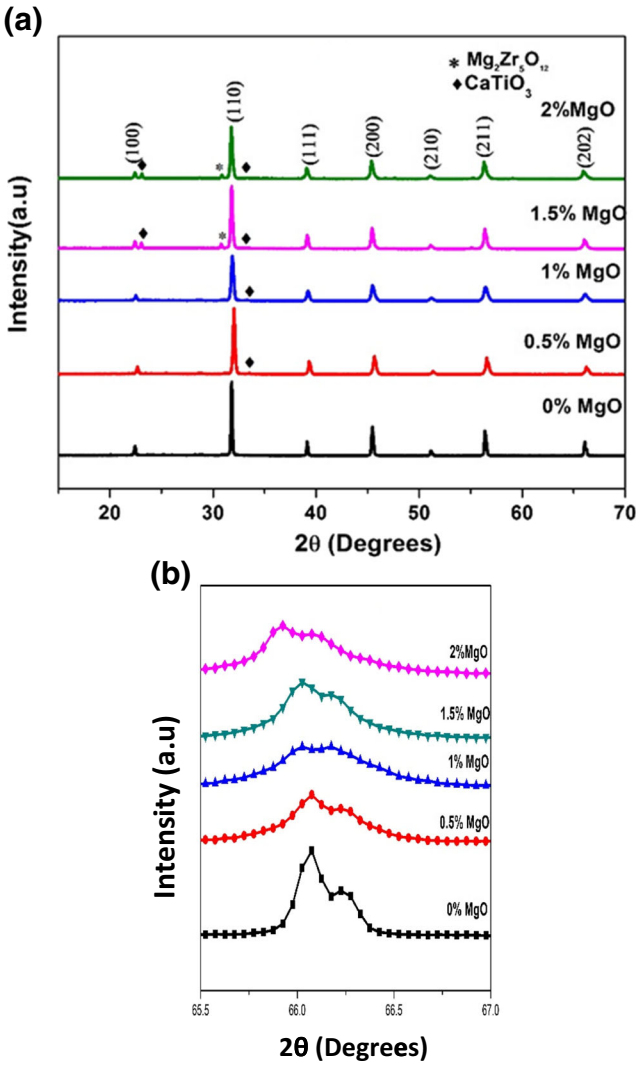

Fig. 2 (**a**) X-ray diffraction patterns of pure BZT-0.5BCT and different vol.% of nano- MgO added sample sintered at 1350 °C/4 h (**b**) magnified X-ray diffraction patterns in the range of 65-67°

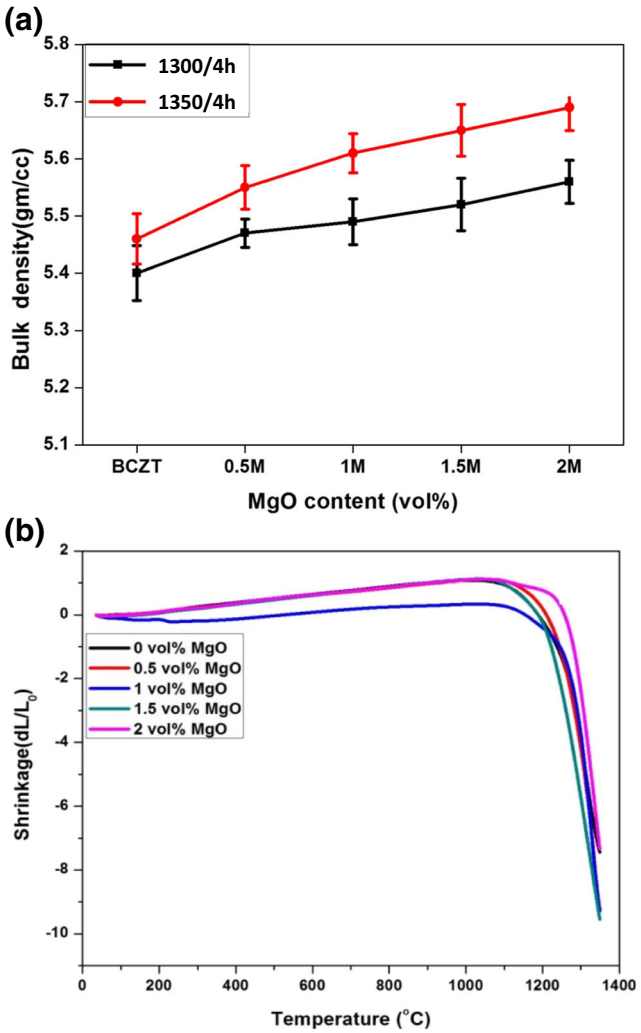

Fig. 3 (**a**) Bulk density of nano-MgO added BZT-0.5BCT sintered at two different temperatures (**b**) Thermal shrinkage of nano-MgO added BZT-0.5BCT from room temperature to 1350 °C

Figure 3 (a) depicts the effect of MgO addition on the sintered density of the BZT-0.5BCT at two sintering temperatures, viz., 1300 °C and 1350 °C. From the figure, it is evident that the bulk density increased marginally with an increase in MgO addition. Thermal shrinkage increases with increase in MgO addition (Fig.3(b)), indicating that MgO incorporation effectively modifies the grain surfaces and promotes densification.

Figure 4 (a-e) shows the microstructure of different vol% MgO added BZT-0.5BCT ceramic sintered at 1350 °C for a dwelling time of 4 h. The grain size was evaluated from the FESEM images using the line intercept method in which a minimum of 30 grains were considered for calculating the average grain size. The values are listed in Table 1. In the FESEM image for the BZT-0.5BCT, Fig. 4 (a), the contrasts of the grains are almost same. A considerable homogeneity of the microstructure is observed. A typical dense microstructure of pure BCZT ceramic with grain to grain contact is revealed in the microstructure. Average grain size of ~4 μm is observed for pure BCZT ceramic. Interestingly, with MgO addition the grain size decreases drastically (Fig.4 [b-e]). Probably, MgO addition, up to a certain level, inhibits grain growth and helps in densification. Sakabe et al. and Park et al. observed grain size reduction in MgO doped $BaTiO_3$ [30, 31]. Also, extra phases with dark contrast are observed in the FESEM image for MgO added sample. EDX analysis of the dark contrast region of 1 Vol% MgO-added BZT-0.5BCT has been studied. Qualitative EDX analysis has revealed that the dark grains exhibit (see Fig. 4) a high calcium concentration, whereas low calcium was detected in the lighter areas. According to the previous XRD analyses, the $CaTiO_3$ phase was detected above 0.5 Vol% MgO additions, which also validates the EDX observation. Thus, the additional phase was assigned as $CaTiO_3$ for a lower amount of MgO addition (0.5–1 vol%).

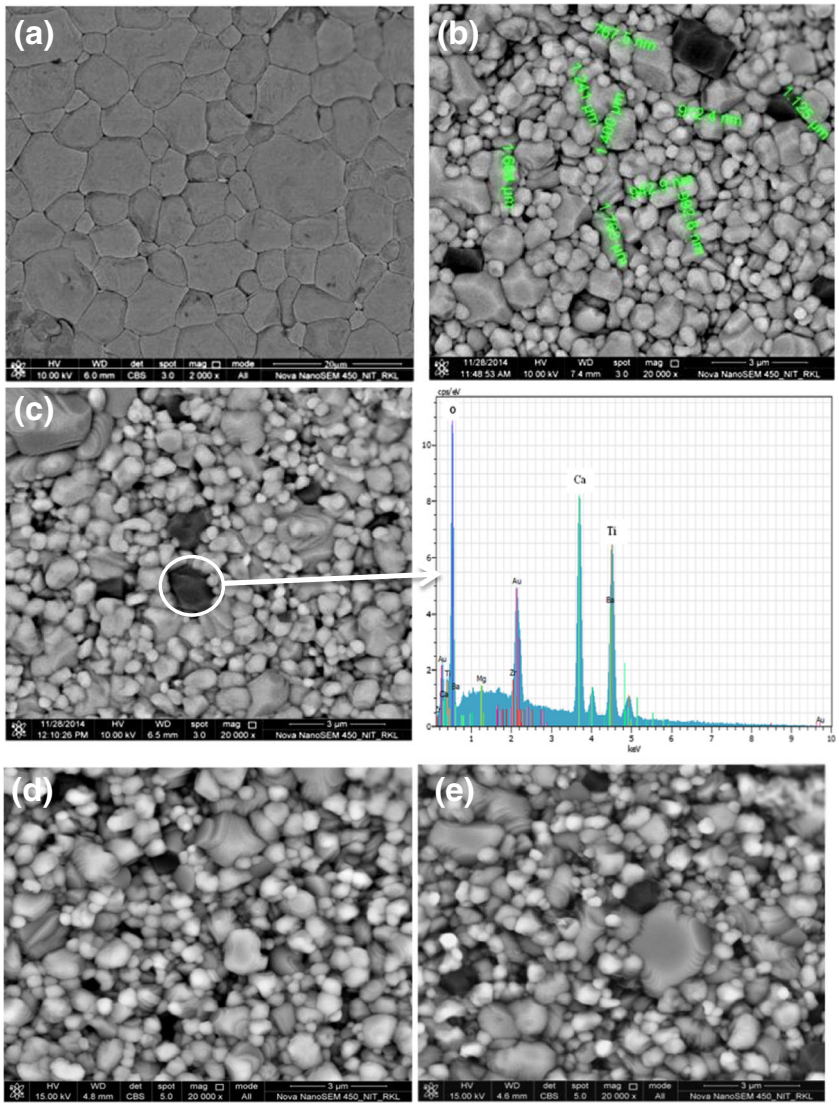

Fig. 4 FESEM micrographs of nano MgO added BZT-0.5BCT ceramic sintered at 1350 °C/4 h (**a**) x = 0 (**b**)x = 0.5 (**c**) x = 1 (**d**) x = 1.5 (**e**) 2 vol%

Figure 5 shows the (a) relative permittivity, and (b) dissipation factor vs. frequency for different MgO added BZT-0.5BCT samples (at room temperature). It can be observed that the room temperature relative permittivity values for MgO added BCZT samples 0, 0.5, 1, 1.5, 2 are 4215, 2842, 2821, 2865 and 2640 respectively at 1 kHz. The loss factor of all BCZT ceramics are less than 2.5 % at 1 kHz, and it decreases with MgO addition. It is to be mentioned that domain wall mobility allows domains to align with an applied external field, yielding extrinsic permittivity contributions. If domains are immobile or less mobile, they cannot contribute or cannot contribute as greatly and thus permittivity is decreased. The most interesting aspect of MgO added samples is its relative permittivity vs. temperature response (Fig.6). It is clear that MgO additions effectively suppress the relative permittivity around phase transition temperature. The phase transformations of $BaTiO_3$ were reported to be

Table 1 Various mechanical and electrical properties of BZT-0.5BCT + MgO sintered specimens

MgO content	Average grain size (Min. - Max.)(Avg.) (μm)	H_v (MPa)	Flexural strength (MPa)	tanδ	ε_r	d_{33} (pC/N)
0	2.85–12 (6.5)	561	73.5	0.0205	4215	450
0.5	0.3–2.2 (0.75)	608	75.55	0.0142	2842	218
1	0.23–1.1 (0.563)	681	92.35	0.0131	2821	126
1.5	0.36–1.35 (0.37)	807.2	93.4	0.0106	2865	16
2	0.3–2.5 (0.35)	630.9	105	0.0160	2640	11

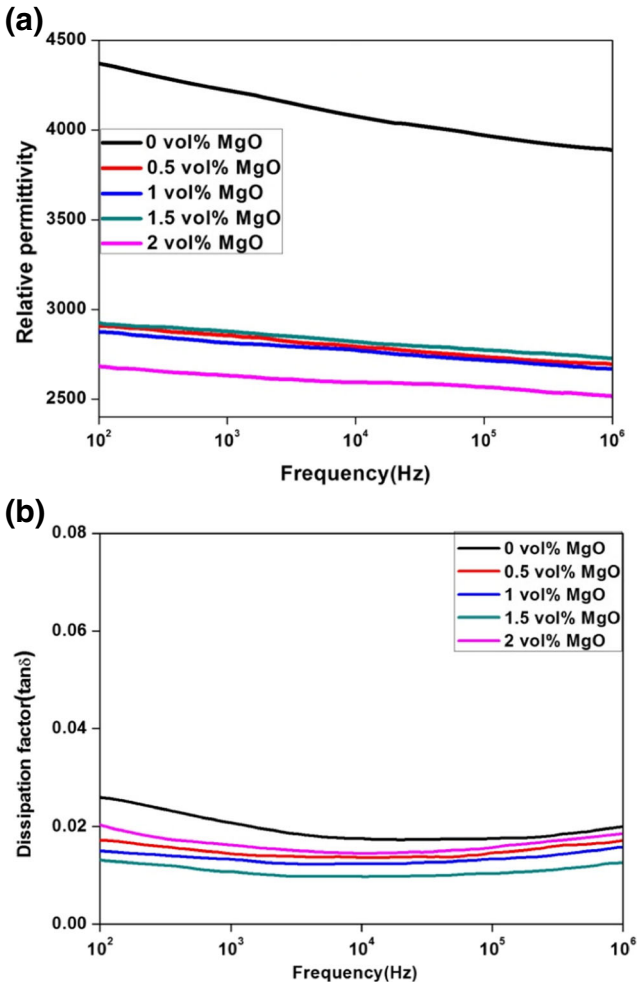

Fig. 5 (**a**) Relative permittivity and (**b**) dissipation factor as the function of frequency for nano-MgO added BZT-0.5BCT ceramic sintered at 1350 °C/4 h

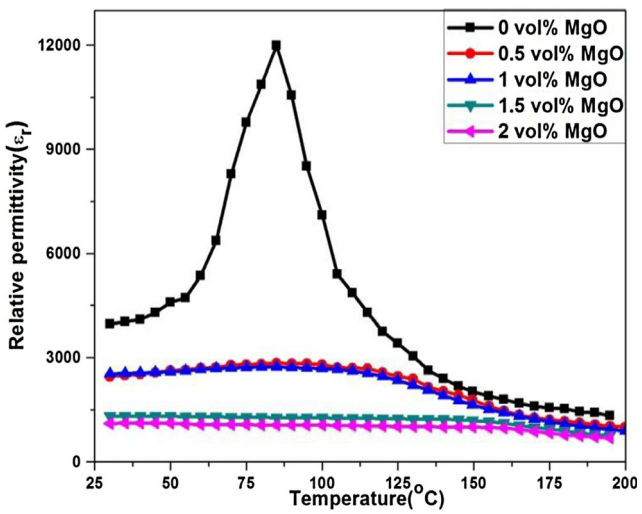

Fig. 6 Temperature dependence of relative permittivity of MgO added BZT-0.5BCT ceramics

changed by the grain size. When the grain size of $BaTiO_3$ is reduced below 1 μm, the tetragonality (*c/a*) of the $BaTiO_3$ phase starts to decrease, and the phase transformations are affected by the "size effect" [32]. In our case reduction in permittivity and flattened phase transition peak could be attributed to the significant reduction in grain size and generation of non-ferroelectric phase in the matrix.

Figure 7 shows the polarization-electric field characterization of the MgO added BZT-0.5BCT ceramics at room temperature. Pure BZT-0.5BCT ceramics is typically soft, with a very low coercive field E_c = 1.2 kV/cm and a relatively high remnant polarization $P_r = 4\mu C/cm^2$. It is found that the remnant polarization (P_r) and coercive fields (E_c) decreases rapidly with increasing MgO content. With the increasing MgO content, the ferroelectric behavior reduces. The decrease in remnant polarization can be attributed to the formation of

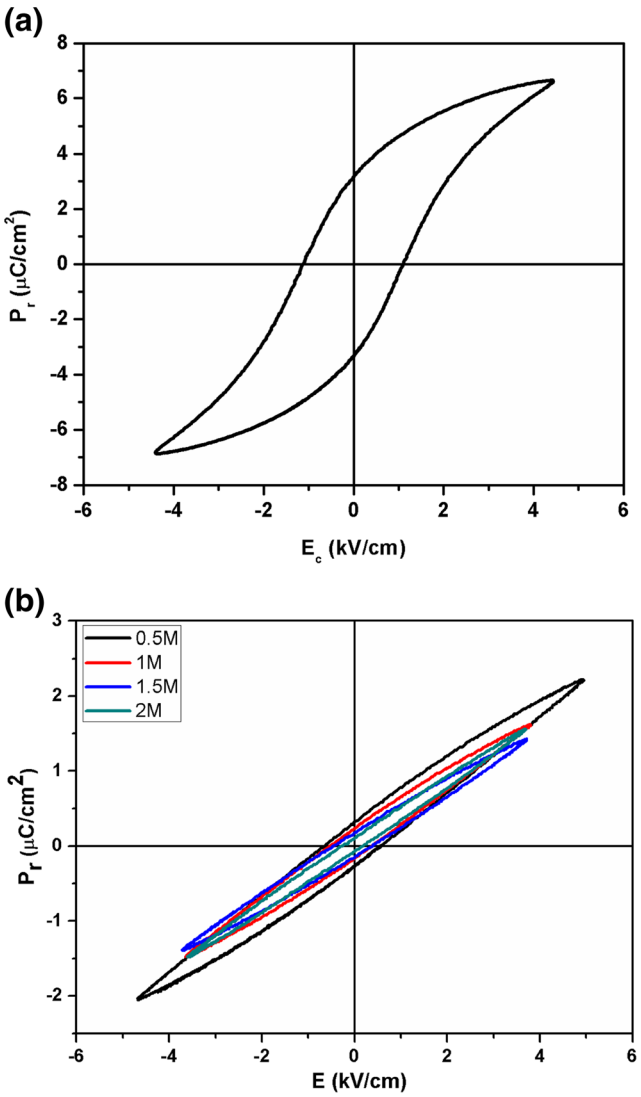

Fig. 7 P-E hysteresis loops of (**a**) BZT-0.5BCT ceramics (**b**) MgO added (0.5–2 vol%) BZT-0.5BCT ceramics at room temperature

non-ferroelectric phase ($CaTiO_3$, MgO-rich phase) and decrease in grain size.

The piezoelectric coefficient (d_{33}) value of MgO added BZT-0.5BCT ceramics is shown in Fig. 8 (a). The d_{33} value sharply decreases with increase in MgO addition. The d_{33} of 126 pC/N was obtained for 1 vol% of MgO addition, which was 66 % less than that of BZT-0.5BCT (450pC/N). For higher concentration of MgO content (beyond 1vol %), piezoelectric constant degrades rapidly, and this is because of non-piezoelectric MgO-rich phase in the matrix. It is accepted that grain size is the main influence on the piezoelectric properties of PZT or $BaTiO_3$–based ceramics. Therefore, in our case, it is likely that the reduction in the piezoelectric properties was mainly due to the reduction in grain size and introduction of non-piezoelectric $CaTiO_3/Mg_2ZrO_4$ phase in the composite ceramics.

The d_{33} value decreases with increase in time (no of hours) as shown in Fig. 8 (b). The aging rate observed for BZT-0.5BCT is 14 %/decade. MgO addition reduces the aging rate. For 1 and 2 vol% MgO added, BZT-0.5BCT shows aging rate of 3 % and 1.5 %/decade. The defect dipole reorientation model is predominant in the acceptor-doped ferroelectric materials, which contain a significant concentration of oxygen vacancies and corresponding defect dipoles to provide sufficient resistance to the domain wall motion. It is also known that drift of charge carriers to the domain walls creating pinning centers and decreasing wall mobility; reorientation of the defect dipoles in the bulk of the domains along the direction of local remnant polarization [33]. This may be the possible reason for the reduction of aging rate in BZT-0.5BCT/MgO composite ceramic. Su et al. [34] observed the extremely high aging rate in BZT-0.5BCT ceramics, 30 % and 25 % loss for d_{33} and kp, respectively, 10^4 min after poling. However, in the present case, further studies are required to understand the exact aging mechanism in MgO added BZT-0.5BCT.

Figure 9 (a) and (b) shows flexural strength and hardness of MgO added BZT-0.5BCT ceramics, respectively. It was found that the hardness and flexural strength, both

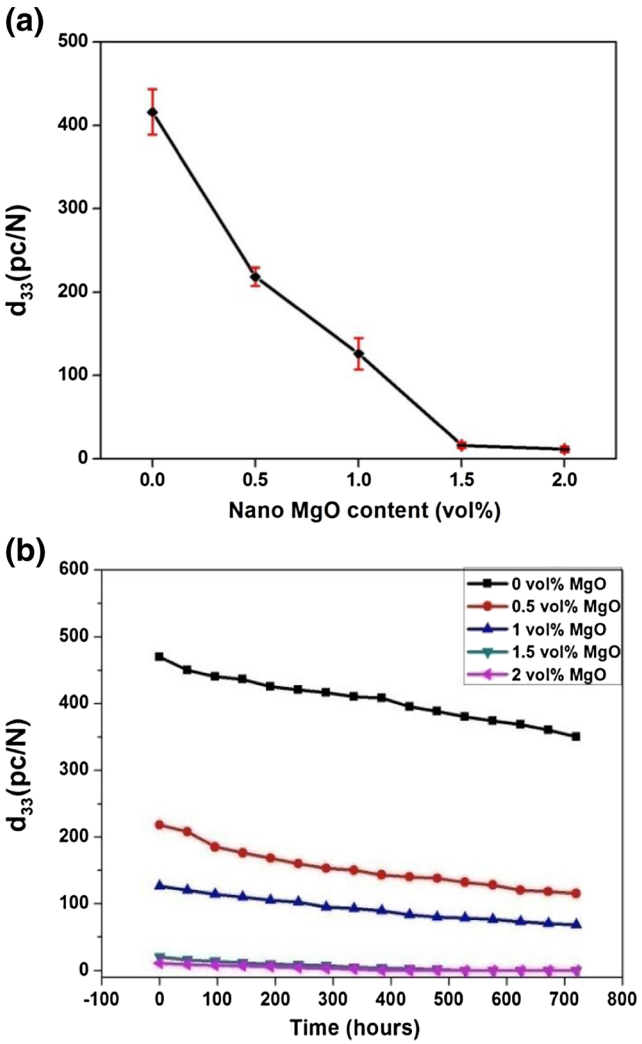

Fig. 8 Variation of piezoelectric coefficient (d_{33}) of sintered BZT-0.5BCT ceramics with (**a**) different vol% of nano oxide (MgO) addition (**b**) time (hours)

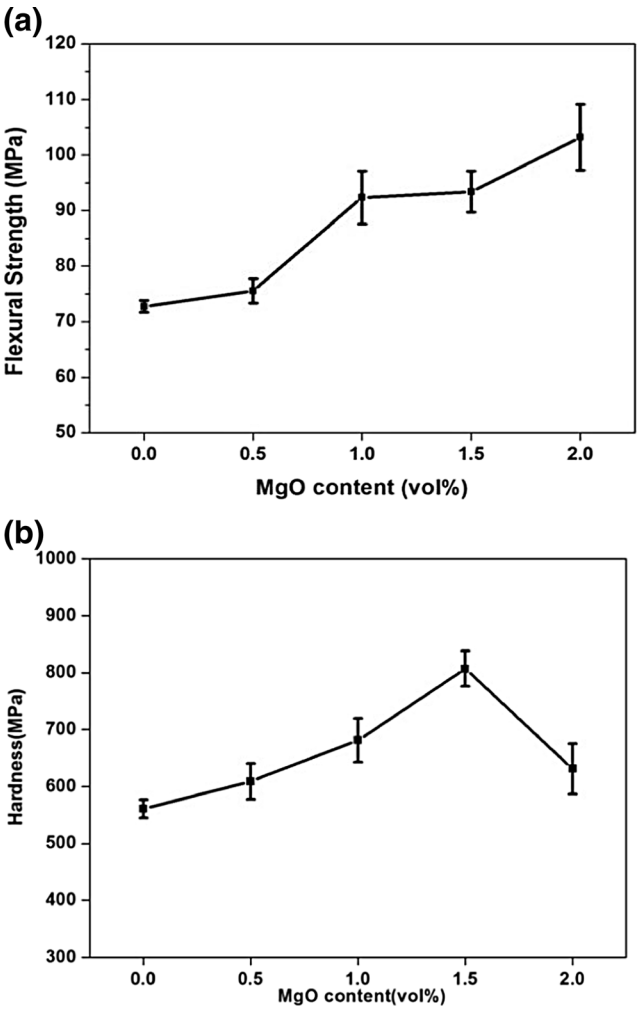

Fig. 9 (**a**) Flexural Strength and (**b**) Hardness of MgO added BZT-0.5BCT ceramics

increases with increase in MgO concentration. In particular, the value of flexural strength of BCZT/1 vol.% MgO was 93 MPa, which is almost 25 % higher than that of monolithic BCZT (73 MPa). Firstly the improved density (Fig. 3[a]) is helpful for enhancing the hardness of the MgO - BZT-0.5BCT composite ceramics. Secondly, non-primary particles precipitated from a supersaturated solid solution may be partly contributing to the strengthening. Classically, high values of H_v are considered to be related to the effect of increased grain boundaries [35] which are found in samples with smaller grain sizes, providing additional obstacles for the movement of lattice dislocations in the adjacent grains, thus leading to harder materials. Further studies are required to understand the decrement of hardness at 2 vol% addition

The BZT-0.5BCT with a flat surface and no clear grain boundaries revealed that the fracture mode was mainly intragranular (Fig.10 [a]). While in MgO added BZT-0.5BCT sample it was intergranular i.e. crack has propagated through the grain boundary (a three-dimensional effect is there) (Fig.10 (b) & (c)). MgO addition significantly reduces the grain size, and the fracture mode also modifies. Also, similar results were reported in PZT/MgO, PZT/ZrO_2 and Al_2O_3/SiC, composite systems by other researchers [36–38]. In summary, the grain size reduction with increasing MgO content (Fig. 4), observed in our BZT-0.5BCT/MgO composite ceramics, is believed to be the major factor influencing the hardening and increase in strength of the composite ceramics.

1 vol% of MgO added sample may be suitable for capacitor application due to flat permittivity-temperature response with reasonably high permittivity (~2800) and improved mechanical strength. Although the d_{33} value decreases with the nano-MgO addition, BZT-0.5BCT containing 0.5–1 vol.% MgO can be used as a cost-effective substitute of pure PZT for low-end applications due to the very low temperature coefficient of permittivity, better mechanical property and low aging rate of d_{33}.

Table 2 summarizes the electrical and mechanical properties of our sample along with the reported data for BZT-0.5BCT and different PZT ceramics for comparison. It is seen from Table 2 that the dielectric, piezoelectric and mechanical properties of our samples are comparable to that of pure PZT and some commercial grade PZT.

4 Conclusions

The addition of MgO in the range of (0–2 vol%) was found to promote densification and reduces grain size significantly. It was observed that addition of MgO more than 0.5 vol% addition produces impurity phases in BZT-0.5BCT. The MgO addition also provided materials with superior mechanical properties

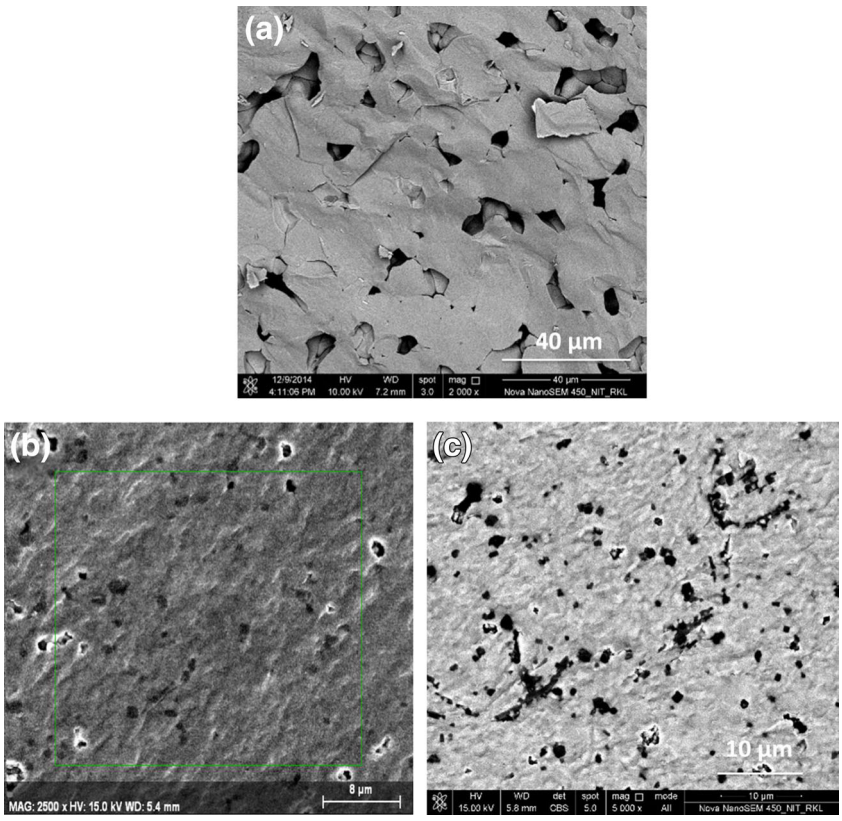

Fig. 10 Fracture surface of BZT-0.5BCT/MgO sintered specimen with different volume percent of MgO (**a)** 0 %, (**b)** 1 % (**c)** 2 %

Table 2 Electrical and mechanical properties of pure and modified BZT-0.5BCT and PZT

Composition	ε_r at RT	% change in ε_r (RT to 80 °C)	d_{33} (pC/N)	Ageing of d_{33} (%/decade)	Macrohardness H_v (GPa)	Flexural strength (MPa)	References
BZT-0.5BCT	3557	375	-	-	0.54	-	Kaushal et al. [14]
BZT-0.5BCT-1.0Al_2O_3	3630	177	380	–7	0.74	92	Prativa et al. [24]
PZT	730[a]	25[a]	223[a] k_p = 0.51	-	0.98[c]	70[b]	[a]Jaffe et al. [1], [b]Pfemer et al. [39], Sharma et al. [40]
PZT-4	1400	27	225–290	–3.5	-	95.2	Hooker et al. [41] http://www.morgantechnicalceramics.com/products [42]
PZT-1.0MgO	927	-	k_p = 0.21	-	3.8[*]	92	Tajima et al. [20]
BZT-0.5BCT	4215	300	450	–14	0.56	73.5	Present work
BZT-0.5BCT-0.5MgO	2842	2	218	–5	0.61	75.55	Present work
BZT-0.5BCT-1.0MgO	2821	2	126	–3	0.68	92.35	Present work

[*] Microhardness, RT = Room Temperature, k_p = Electromechanical coupling coefficient

but degrades the dielectric and piezoelectric properties. The most interesting aspect of MgO added samples is their relative permittivity vs temperature response. It is clear that MgO additions effectively suppress the relative permittivity around phase transition temperature. In this case reduction in permittivity and flattened phase transition peak could be attributed to the significant reduction in grain size and generation of non-ferroelectric phase in the matrix. 0.5–1 vol% of MgO added sample may be suitable for capacitor application due to flat permittivity-temperature response with reasonably high permittivity (~2800) and improved mechanical strength. The same composition also can be used as a cost-effective substitute of pure PZT for low-end applications due to improved mechanical property, reasonable d_{33} (218 pC/N) and low aging rate of d_{33}.

References

1. B. Jaffe, W. R. Cook, and H. Jaffe, Piezoelectric Ceramics, Academic Press, (1971).
2. K. Uchino, *Ferroelectric Devices* (Marcel Dekker Inc, New York, 2000)
3. A. J. Moulson, J. M. Herbert, *Electroceramics: Materials, Properties, Applications,* (Chapman & Hall, London, 1990)
4. Y. Saito, H. Takao, T. Tani, T. Nonoyama, K. Takatori, T. Homma, T. Nagaya, M. Nakamura, Nature **432**, 84 (2004)
5. M. E. Rogers, C. M. Fancher, J. E. Blendell, Journal of Applied Physics **112**, 052014 (2012)
6. D. Y. Wang, N. Y. Chan, S. Li, S. H. Choy, H. Y. Tian, H. L. W. Chan, Applied Physics Letters **97**, 212901 (2010)
7. K. I. Park, S. Xu, Y. Liu, G. T. Hwang, S. J. L. Kang, Z. L. Wang, K. J. Lee, Nano Letters **10**, 4939 (2010)
8. Y. C. Yang, C. Song, X. H. Wang, F. Zeng, F. Pan, Applied Physics Letters **92**, 012907 (2008)
9. D. M. Lin, D. Q. Xiao, J. G. Zhu, P. Yu, Applied Physics Letters **88**, 062901 (2006)
10. W. F. Liu, X. B. Ren, Physical Review Letters **10**, 3257602 (2009)
11. W. Li, Z. Xun, R. Chu, P. Fu, G. Zang, Physica B **405**, 4513 (2010)
12. P. Wang, Y. Li, and Y. Lu, Journal of the European Ceramic Society, 31**,** 2005, (2011).
13. F. Benabdallah, A. Simon, H. Khemakhem, C. Elissalde, M. Maglione, Journal of Applied Physics **109**, 124116 (2011)
14. A. Kaushal, S. M. Olhero, B. Singh, R. Zamiri, V. Saravanan and J. M. F. Ferreira, RSC Adv., **4**, 26993, (2014),
15. A. Srinivasa, R. V. Krishnaiaha, V. L. Niranjania, S. V. Kamata, T. Karthik, S. Asthana, Ceramics International **41**, 1980–1985 (2015)
16. S. Jiansirisomboon, A. Watcharapasorn, Current Applied Physics **8**, 48 (2008)
17. H. J. Hwang, M. Toriyama, T. Sekino, K. Niihara, J. Euro, Ceram. Soc **18**, 2193 (1998)
18. H. Hyuga, Y. Hayashi, T. Sekino, K. Niihara, Nanostructured Materials **9**, 547 (1997)
19. C. Y. Chen, W. H. Tuan, Journal of Materials Science Letters **18**, 353 (1999)
20. K. Tajima, H. J. Hwang, M. Sandoand, K. Niihara, Journal of the European Ceramic Society **19**, 1179 (1999)
21. S. Jiansirisomboon, M. Promsawat, O. Namsar, A. Watcharapasorn, Materials Chemistry and Physics **117**, 80 (2009)

22. T. Zeng, X. Dong, H. Yang, C. Mao, H. Chen, Scripta Mater **55**, 923 (2006)
23. P. Xiang, X. Dong, H. Chen, Z. Zhang, J. Guo, Ceram. Inter **29**, 499–503 (2003)
24. P. Adhikari, R. Mazumder, G. K. Sahoo, Ferroelectrics **490**, 60–69 (2016)
25. P. Ren, H. Fan, X. Wang, X. Tan, Materials Research Bulletin **46**, 2308 (2011)
26. T. Nagai, K. Iijim, H. Hwang, M. Sando, T. Sekino and K. Niihara, Journal of the American Ceramic Society, 83 (1), 107, (2000).
27. S. Yoon, J. Lee, D. Kim and N. M. Hwang, Journal of the American Ceramic Society, 86 (1), 88, (2003).
28. W. C. Vittayakorn, D. Bunjong, R. Muanghlua, N. Vittayakorn, J. Ceram, Process. Res **12**(5), 493–495 (2011)
29. ASTM C1161–90, Standard test method for flexural strength of advanced ceramics at ambient temperature, Annual Book of ASTM Standards, Vol. 15**.01**. ASTM, pp. 327–333 (1991).
30. Y. Sakabe, N. Wada, T. Hiramatsu, T. Tonogaki, Japanese Journal of Applied Physics **41**, 6922 (2002)
31. J. S. Park, Y. H. Han, Journal of the European Ceramic Society **27**, 1077 (2007)
32. K. Uchino, E. Sadanaga, T. Hirose, J. Am, Ceram.Soc **72**(8), 1555–1989
33. J. R. Scholz "Aging Rates in PZT Ferroelectrics with Mixed Acceptor-Donor Dopants" MS thesis, Pennsylvania State University, (2009).
34. S. Su, R. Zuo, S. Lu, Z. Xu, X. Wang, L. Li, Curr. App. Phys **11**, S120 (2011)
35. S. J. Jeong, J. B. Kim, Integrated Ferroelectrics **90**, 12 (2007)
36. K. L. Kendig, D. B. Miracle, Acta Materialia **50**, 4165 (2002)
37. K. Niihara, Journal of the Ceramic Society of Japan **99**, 974 (1991)
38. Y. Wu, T. Feng, J. Alloys, Comp **491**, 452 (2010)
39. R. A. Pferner, G. Thurn, F. Aldinger, Materials Chemistry and Physics **61**, 24–30 (1999)
40. P. K. Sharma, Z. Ounaies, V. V. Varadan, V. K. Varadan, Smart Materials and Structures **10**, 878–883 (2001)
41. M. W. Hooker, NASA / CR- 1998–208708
42. http://www.morgantechnicalceramics.com/products/